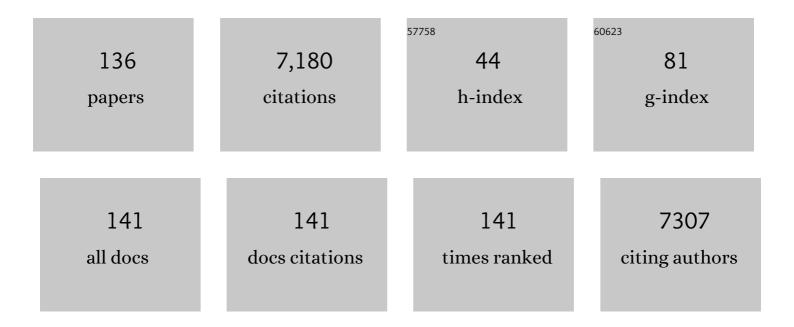
Paul Fenter

List of Publications by Year in descending order

Source: https://exaly.com/author-pdf/5589184/publications.pdf Version: 2024-02-01



DALL FENTED

#	Article	IF	CITATIONS
1	Understanding the Solid-State Electrode–Electrolyte Interface of a Model System Using First-Principles Statistical Mechanics and Thin-Film X-ray Characterization. ACS Applied Materials & Interfaces, 2022, 14, 7428-7439.	8.0	1
2	Structural Changes during the Conversion Reaction of Tungsten Oxide Electrodes with Tailored, Mesoscale Porosity. ACS Nano, 2022, 16, 5384-5392.	14.6	6
3	Emergent Behavior at the Calcite–Water Interface during Reactive Transport in a Simple Microfluidic Channel. ACS Earth and Space Chemistry, 2022, 6, 861-870.	2.7	4
4	Density Functional Tight-Binding Simulations Reveal the Presence of Surface Defects on the Quartz (101)–Water Interface. Journal of Physical Chemistry C, 2021, 125, 16246-16255.	3.1	4
5	The Patterson function as auto-hologram and graph enables the direct solution to the phase problem for coherently illuminated atomistic structures. New Journal of Physics, 2021, 23, 073018.	2.9	0
6	Ion correlations drive charge overscreening and heterogeneous nucleation at solid–aqueous electrolyte interfaces. Proceedings of the National Academy of Sciences of the United States of America, 2021, 118, .	7.1	28
7	Probing the <i>In Situ</i> Pseudocapacitive Charge Storage in Ti ₃ C ₂ MXene Thin Films with X-ray Reflectivity. ACS Applied Materials & Interfaces, 2021, 13, 43597-43605.	8.0	8
8	Pore-Scale Oil Connectivity and Displacement by Controlled-Ionic-Composition Waterflooding Using Synchrotron X-Ray Microtomography. SPE Journal, 2021, 26, 3694-3701.	3.1	4
9	Replacement of Calcium Carbonate Polymorphs by Cerussite. ACS Earth and Space Chemistry, 2021, 5, 2433-2441.	2.7	9
10	Tailoring Interfaces in Solid-State Batteries Using Interfacial Thermochemistry and Band Alignment. Chemistry of Materials, 2021, 33, 8447-8459.	6.7	7
11	Pb Sorption at the Barite (001)–Water Interface. Journal of Physical Chemistry C, 2020, 124, 22035-22045.	3.1	9
12	Pore Scale Investigation of Oil Displacement Dynamics by Smart Waterflooding using Synchrotron X-ray Microtomography. , 2020, , .		2
13	Molecular-scale origins of wettability at petroleum–brine–carbonate interfaces. Scientific Reports, 2020, 10, 20507.	3.3	5
14	Direct recovery of interfacial topography from coherent X-ray reflectivity: model calculations for a 1D interface. Acta Crystallographica Section A: Foundations and Advances, 2020, 76, 458-467.	0.1	3
15	Nonclassical Behavior in Competitive Ion Adsorption at a Charged Solid–Water Interface. Journal of Physical Chemistry Letters, 2020, 11, 4029-4035.	4.6	10
16	Validating first-principles molecular dynamics calculations of oxide/water interfaces with x-ray reflectivity data. Physical Review Materials, 2020, 4, .	2.4	12
17	Nonreciprocal interactions induced by water in confinement. Physical Review Research, 2020, 2, .	3.6	29
18	Microscale Investigation of Dynamic Wettability Alteration Effect on Oil Displacement by Smart Waterflooding Using Synchrotron-Based Microtomography. , 2020, , .		3

#	Article	IF	CITATIONS
19	Epitaxial Growth of Gibbsite Sheets on the Basal Surface of Muscovite Mica. Journal of Physical Chemistry C, 2019, 123, 27615-27627.	3.1	10
20	Effect of Anions on the Changes in the Structure and Adsorption Mechanism of Zirconium Species at the Muscovite (001)–Water Interface. Journal of Physical Chemistry C, 2019, 123, 16699-16710.	3.1	7
21	Understanding the Role of Overpotentials in Lithium Ion Conversion Reactions: Visualizing the Interface. ACS Nano, 2019, 13, 7825-7832.	14.6	16
22	Mapping Three-dimensional Dissolution Rates of Calcite Microcrystals: Effects of Surface Curvature and Dissolved Metal Ions. ACS Earth and Space Chemistry, 2019, 3, 833-843.	2.7	40
23	Structural analysis of the initial lithiation of NiO thin film electrodes. Physical Chemistry Chemical Physics, 2019, 21, 8897-8905.	2.8	13
24	Effect of pH on the Formation of Gibbsite-Layer Films at the Muscovite (001)–Water Interface. Journal of Physical Chemistry C, 2019, 123, 6560-6571.	3.1	14
25	Oxidation induced strain and defects in magnetite crystals. Nature Communications, 2019, 10, 703.	12.8	40
26	Dissolution Kinetics of Epitaxial Cadmium Carbonate Overgrowths on Dolomite. ACS Earth and Space Chemistry, 2019, 3, 212-220.	2.7	3
27	Simultaneous Adsorption and Incorporation of Sr ²⁺ at the Barite (001)–Water Interface. Journal of Physical Chemistry C, 2019, 123, 1194-1207.	3.1	21
28	Cathodic Corrosion at the Bismuth–Ionic Liquid Electrolyte Interface under Conditions for CO ₂ Reduction. Chemistry of Materials, 2018, 30, 2362-2373.	6.7	38
29	Evolution of Strain in Heteroepitaxial Cadmium Carbonate Overgrowths on Dolomite. Crystal Growth and Design, 2018, 18, 2871-2882.	3.0	6
30	Mechanistic understanding of tungsten oxide in-plane nanostructure growth <i>via</i> sequential infiltration synthesis. Nanoscale, 2018, 10, 3469-3479.	5.6	25
31	Pulsed Laser Deposition and Characterization of Heteroepitaxial LiMn ₂ O ₄ /La _{0.5} Sr _{0.5} CoO ₃ Bilayer Thin Films as Model Lithium Ion Battery Cathodes. ACS Applied Nano Materials, 2018, 1, 642-653.	5.0	18
32	Templating Growth of a Pseudomorphic Lepidocrocite Microshell at the Calcite–Water Interface. Chemistry of Materials, 2018, 30, 700-707.	6.7	4
33	Pb ²⁺ –Calcite Interactions under Far-from-Equilibrium Conditions: Formation of Micropyramids and Pseudomorphic Growth of Cerussite. Journal of Physical Chemistry C, 2018, 122, 2238-2247.	3.1	23
34	Arsenic uptake in bacterial calcite. Geochimica Et Cosmochimica Acta, 2018, 222, 642-654.	3.9	20
35	Effect of nitrogen passivation on interface composition and physical stress in SiO2/SiC(4H) structures. Applied Physics Letters, 2018, 113, .	3.3	12
36	Insights on the Alumina–Water Interface Structure by Direct Comparison of Density Functional Simulations with X-ray Reflectivity. Journal of Physical Chemistry C, 2018, 122, 26934-26944.	3.1	19

#	Article	IF	CITATIONS
37	Strain-Driven Mn-Reorganization in Overlithiated Li _{<i>x</i>} Mn ₂ O ₄ Epitaxial Thin-Film Electrodes. ACS Applied Energy Materials, 2018, 1, 2526-2535.	5.1	18
38	Heteroepitaxial growth of cadmium carbonate at dolomite and calcite surfaces: Mechanisms and rates. Geochimica Et Cosmochimica Acta, 2017, 205, 360-380.	3.9	28
39	Reversible Li-Ion Conversion Reaction for a Ti _{<i>x</i>} Ge Alloy in a Ti/Ge Multilayer. ACS Applied Materials & Interfaces, 2017, 9, 8169-8176.	8.0	14
40	Stern Layer Structure and Energetics at Mica–Water Interfaces. Journal of Physical Chemistry C, 2017, 121, 9402-9412.	3.1	119
41	High Voltage LiNi _{0.5} Mn _{0.3} Co _{0.2} O ₂ /Graphite Cell Cycled at 4.6 V with a FEC/HFDECâ€Based Electrolyte. Advanced Energy Materials, 2017, 7, 1700109.	19.5	98
42	Hydration Structure of the Barite (001)–Water Interface: Comparison of X-ray Reflectivity with Molecular Dynamics Simulations. Journal of Physical Chemistry C, 2017, 121, 12236-12248.	3.1	38
43	Real-time observation of cation exchange kinetics and dynamics at the muscovite-water interface. Nature Communications, 2017, 8, 15826.	12.8	61
44	Investigation of Glutaric Anhydride as an Electrolyte Additive for Graphite/LiNi _{0.5} Mn _{0.3} Co _{0.2} O ₂ Full Cells. Journal of the Electrochemical Society, 2017, 164, A173-A179.	2.9	9
45	Structural Dynamics and Evolution of Bismuth Electrodes during Electrochemical Reduction of CO ₂ in Imidazolium-Based Ionic Liquid Solutions. ACS Catalysis, 2017, 7, 7285-7295.	11.2	41
46	Lithiation of multilayer Ni/NiO electrodes: criticality of nickel layer thicknesses on conversion reaction kinetics. Physical Chemistry Chemical Physics, 2017, 19, 20029-20039.	2.8	17
47	Advanced hybrid battery with a magnesium metal anode and a spinel LiMn ₂ O ₄ cathode. Chemical Communications, 2016, 52, 9961-9964.	4.1	50
48	Polyanthraquinoneâ€Based Organic Cathode for Highâ€Performance Rechargeable Magnesiumâ€ion Batteries. Advanced Energy Materials, 2016, 6, 1600140.	19.5	210
49	Phase control of Mn-based spinel films via pulsed laser deposition. Journal of Applied Physics, 2016, 120, .	2.5	4
50	Morphological Evolution of Multilayer Ni/NiO Thin Film Electrodes during Lithiation. ACS Applied Materials & Interfaces, 2016, 8, 19979-19986.	8.0	26
51	Surface Charge of the Calcite (104) Terrace Measured by Rb ⁺ Adsorption in Aqueous Solutions Using Resonant Anomalous X-ray Reflectivity. Journal of Physical Chemistry C, 2016, 120, 15216-15223.	3.1	24
52	A Comparison of Adsorption, Reduction, and Polymerization of the Plutonyl(VI) and Uranyl(VI) Ions from Solution onto the Muscovite Basal Plane. Langmuir, 2016, 32, 10473-10482.	3.5	8
53	Structural Characterization of Aluminum (Oxy)hydroxide Films at the Muscovite (001)–Water Interface. Langmuir, 2016, 32, 477-486.	3.5	14
54	Dimensionally Controlled Lithiation of Chromium Oxide. Chemistry of Materials, 2016, 28, 47-54.	6.7	18

#	Article	IF	CITATIONS
55	Replacement of Calcite (CaCO ₃) by Cerussite (PbCO ₃). Environmental Science & Technology, 2016, 50, 12984-12991.	10.0	51
56	Understanding Defect‣tabilized Noncovalent Functionalization of Graphene. Advanced Materials Interfaces, 2015, 2, 1500277.	3.7	19
57	Phase-Controlled Electrochemical Activity of Epitaxial Mg-Spinel Thin Films. ACS Applied Materials & Interfaces, 2015, 7, 28438-28443.	8.0	56
58	Rb ⁺ Adsorption at the Quartz(101)–Aqueous Interface: Comparison of Resonant Anomalous X-ray Reflectivity with ab Initio Calculations. Journal of Physical Chemistry C, 2015, 119, 4778-4788.	3.1	34
59	Interfacial ionic â€~liquids': connecting static and dynamic structures. Journal of Physics Condensed Matter, 2015, 27, 032101.	1.8	67
60	Effects of the background electrolyte on Th(IV) sorption to muscovite mica. Geochimica Et Cosmochimica Acta, 2015, 165, 280-293.	3.9	11
61	Improving Electrodeposition of Mg through an Open Circuit Potential Hold. Journal of Physical Chemistry C, 2015, 119, 23366-23372.	3.1	19
62	X-ray–driven reaction front dynamics at calcite-water interfaces. Science, 2015, 349, 1330-1334.	12.6	69
63	Full-field X-ray reflection microscopy of epitaxial thin-films. Journal of Synchrotron Radiation, 2014, 21, 1252-1261.	2.4	41
64	Hydration layer structure at solid–water interfaces. MRS Bulletin, 2014, 39, 1056-1061.	3.5	65
65	Lithium Intercalation Behavior in Multilayer Silicon Electrodes. Advanced Energy Materials, 2014, 4, 1301494.	19.5	35
66	Electrodes: Lithium Intercalation Behavior in Multilayer Silicon Electrodes (Adv. Energy Mater.) Tj ETQq0 0 0 rgB	「/Qyerloch 19:5	۶ 10 Tf 50 30
67	Structural Origins of Potential Dependent Hysteresis at the Electrified Graphene/Ionic Liquid Interface. Journal of Physical Chemistry C, 2014, 118, 569-574.	3.1	111
68	Atomic Layer Deposition of Gallium Sulfide Films Using Hexakis(dimethylamido)digallium and Hydrogen Sulfide. Chemistry of Materials, 2014, 26, 1029-1039.	6.7	79
69	Incorporation of Pb at the Calcite (104)–Water Interface. Environmental Science & Technology, 2014, 48, 9263-9269.	10.0	46
70	On the variation of dissolution rates at the orthoclase (0 0 1) surface with pH and temperature. Geochimica Et Cosmochimica Acta, 2014, 141, 598-611.	3.9	16
71	Surface-Mediated Formation of Pu(IV) Nanoparticles at the Muscovite-Electrolyte Interface. Environmental Science & Technology, 2013, 47, 14178-14184.	10.0	27
72	Changes in adsorption free energy and speciation during competitive adsorption between monovalent cations at the muscovite (001)-water interface. Geochimica Et Cosmochimica Acta, 2013, 123, 416-426.	3.9	57

#	Article	IF	CITATIONS
73	Optimizing a flow-through X-ray transmission cell for studies of temporal and spatial variations of ion distributions at mineral–water interfaces. Journal of Synchrotron Radiation, 2013, 20, 125-136.	2.4	17
74	Is the Calcite–Water Interface Understood? Direct Comparisons of Molecular Dynamics Simulations with Specular X-ray Reflectivity Data. Journal of Physical Chemistry C, 2013, 117, 5028-5042.	3.1	148
75	Investigation of Structure, Adsorption Free Energy, and Overcharging Behavior of Trivalent Yttrium Adsorbed at the MuscoviteÂ(001)–Water Interface. Journal of Physical Chemistry C, 2013, 117, 23738-23749.	3.1	36
76	APPLICATIONS OF XSW IN INTERFACIAL GEOCHEMISTRY. Series on Synchrotron Radiation Techniques and Applications, 2013, , 369-377.	0.2	0
77	XSW IMAGING. Series on Synchrotron Radiation Techniques and Applications, 2013, , 289-302.	0.2	2
78	Surface diffraction on a l̈-circle diffractometer using the l̈‡-axis geometry. Journal of Applied Crystallography, 2013, 46, 639-643.	4.5	5
79	Interfacial Bonding and Structure of <mml:math <br="" xmlns:mml="http://www.w3.org/1998/Math/MathML">display="inline" > <mml:msub> <mml:mi> Bi </mml:mi> <mml:mn> 2 </mml:mn> </mml:msub> <mml:msub> <mml:mi Insulator Films on Si(111) Determined by Surface X-Ray Scattering. Physical Review Letters, 2013, 110, 226103.</mml:mi </mml:msub></mml:math>	>Te7.8	:mi> <mml:mi 11</mml:mi
80	Understanding controls on interfacial wetting at epitaxial graphene: Experiment and theory. Physical Review B, 2012, 85, .	3.2	95
81	Adsorption of Plutonium Oxide Nanoparticles. Langmuir, 2012, 28, 2620-2627.	3.5	27
82	Nanoscale Perturbations of Room Temperature Ionic Liquid Structure at Charged and Uncharged Interfaces. ACS Nano, 2012, 6, 9818-9827.	14.6	151
83	Monovalent Ion Adsorption at the Muscovite (001)–Solution Interface: Relationships among Ion Coverage and Speciation, Interfacial Water Structure, and Substrate Relaxation. Langmuir, 2012, 28, 8637-8650.	3.5	128
84	Real-Time Observations of Interfacial Lithiation in a Metal Silicide Thin Film. Journal of Physical Chemistry C, 2012, 116, 22341-22345.	3.1	29
85	Sorption of tetravalent thorium on muscovite. Geochimica Et Cosmochimica Acta, 2012, 88, 66-76.	3.9	28
86	Stuffed structures. Nature Materials, 2012, 11, 183-184.	27.5	5
87	Comparison of Cation Adsorption by Isostructural Rutile and Cassiterite. Langmuir, 2011, 27, 4585-4593.	3.5	29
88	Heavy Metal Sorption at the Muscovite (001)–Fulvic Acid Interface. Environmental Science & Technology, 2011, 45, 9574-9581.	10.0	35
89	Application of X-ray reflection interface microscopy to thin-film materials. Nuclear Instruments and Methods in Physics Research, Section A: Accelerators, Spectrometers, Detectors and Associated Equipment, 2011, 649, 188-190.	1.6	2
90	Direct and quantitative comparison of pixelated density profiles with high-resolution X-ray reflectivityAdata. Journal of Synchrotron Radiation, 2011, 18, 257-265.	2.4	18

#	Article	IF	CITATIONS
91	Structural analysis of PTCDA monolayers on epitaxial graphene with ultra-high vacuum scanning tunneling microscopy and high-resolution X-ray reflectivity. Surface Science, 2011, 605, 1685-1693.	1.9	58
92	Electronic structure of lithium battery interphase compounds: Comparison between inelastic x-ray scattering measurements and theory. Journal of Chemical Physics, 2011, 135, 224513.	3.0	39
93	In situ imaging of orthoclase–aqueous solution interfaces with x-ray reflection interface microscopy. Journal of Applied Physics, 2011, 110, 102211.	2.5	8
94	Exploitation of the sorptive properties of mica for the preparation of higher-resolution alpha-spectroscopy samples. Radiochimica Acta, 2010, 98, 431-436.	1.2	11
95	Direct method for imaging elemental distribution profiles with long-period x-ray standing waves. Physical Review B, 2010, 81, .	3.2	9
96	Rb ⁺ and Sr ²⁺ Adsorption at the TiO ₂ (110)â^'Electrolyte Interface Observed with Resonant Anomalous X-ray Reflectivity. Langmuir, 2010, 26, 950-958.	3.5	19
97	Hydrated Cation Speciation at the Muscovite (001)â^ Water Interface. Langmuir, 2010, 26, 16647-16651.	3.5	126
98	Competitive adsorption of strontium and fulvic acid at the muscovite–solution interface observed with resonant anomalous X-ray reflectivity. Geochimica Et Cosmochimica Acta, 2010, 74, 1762-1776.	3.9	47
99	Structure and oxidation state of hematite surfaces reacted with aqueous Fe(II) at acidic and neutral pH. Geochimica Et Cosmochimica Acta, 2010, 74, 1498-1512.	3.9	76
100	Probing interfacial reactions with X-ray reflectivity and X-ray reflection interface microscopy: Influence of NaCl on the dissolution of orthoclase at pOH 2 and 85°C. Geochimica Et Cosmochimica Acta, 2010, 74, 3396-3411.	3.9	14
101	Interaction of muscovite (001) with Pu3+ bearing solutions at pH 3 through ex-situ observations. Geochimica Et Cosmochimica Acta, 2010, 74, 6984-6995.	3.9	15
102	Enhanced Uptake and Modified Distribution of Mercury(II) by Fulvic Acid on the Muscovite (001) Surface. Environmental Science & Technology, 2009, 43, 5295-5300.	10.0	43
103	Water ordering and surface relaxations at the hematite (110)–water interface. Geochimica Et Cosmochimica Acta, 2009, 73, 2242-2251.	3.9	58
104	Image contrast in X-ray reflection interface microscopy: comparison of data with model calculations and simulations. Journal of Synchrotron Radiation, 2008, 15, 558-571.	2.4	23
105	Fulvic Acid Sorption on Muscovite Mica as a Function of pH and Time Using In Situ X-ray Reflectivity. Langmuir, 2008, 24, 7817-7829.	3.5	19
106	Adsorption of Rb+ and Sr2+ at the orthoclase (001)–solution interface. Geochimica Et Cosmochimica Acta, 2008, 72, 1848-1863.	3.9	20
107	Simultaneous inner- and outer-sphere arsenate adsorption on corundum and hematite. Geochimica Et Cosmochimica Acta, 2008, 72, 1986-2004.	3.9	220
108	Bridging arsenate surface complexes on the hematite (012) surface. Geochimica Et Cosmochimica Acta, 2007, 71, 1883-1897.	3.9	103

#	Article	IF	CITATIONS
109	Distribution of barium and fulvic acid at the mica–solution interface using in-situ X-ray reflectivity. Geochimica Et Cosmochimica Acta, 2007, 71, 5763-5781.	3.9	53
110	Interfacial water structure on the (012) surface of hematite: Ordering and reactivity in comparison with corundum. Geochimica Et Cosmochimica Acta, 2007, 71, 5313-5324.	3.9	79
111	Quantitative Lateral Force Microscopy Study of the Dolomite (104)â^Water Interface. Langmuir, 2007, 23, 8909-8915.	3.5	9
112	Electric Double Layer at Metal Oxide Surfaces:Â Static Properties of the Cassiteriteâ^'Water Interface. Langmuir, 2007, 23, 4925-4937.	3.5	63
113	Structure of rutile TiO2 (110) in water and 1molal Rb+ at pH 12: Inter-relationship among surface charge, interfacial hydration structure, and substrate structural displacements. Surface Science, 2007, 601, 1129-1143.	1.9	78
114	Resonant anomalous X-ray reflectivity as a probe of ion adsorption at solid–liquid interfaces. Thin Solid Films, 2007, 515, 5654-5659.	1.8	30
115	Termination and Water Adsorption at the α-Al2O3(012)â^'Aqueous Solution Interface. Langmuir, 2006, 22, 4668-4673.	3.5	99
116	Cation sorption on the muscovite (001) surface in chloride solutions using high-resolution X-ray reflectivity. Geochimica Et Cosmochimica Acta, 2006, 70, 3549-3565.	3.9	182
117	Structure of hydrated Zn2+ at the rutile TiO2 (110)-aqueous solution interface: Comparison of X-ray standing wave, X-ray absorption spectroscopy, and density functional theory results. Geochimica Et Cosmochimica Acta, 2006, 70, 4039-4056.	3.9	52
118	On the use of CCD area detectors for high-resolution specular X-ray reflectivity. Journal of Synchrotron Radiation, 2006, 13, 293-303.	2.4	47
119	Observation of subnanometre-high surface topography with X-ray reflection phase-contrast microscopy. Nature Physics, 2006, 2, 700-704.	16.7	60
120	Inner-sphere adsorption geometry of Se(IV) at the hematite (100)–water interface. Journal of Colloid and Interface Science, 2006, 297, 665-671.	9.4	74
121	Structure of the fluorapatite (100)-water interface by high-resolution X-ray reflectivity. American Mineralogist, 2004, 89, 1647-1654.	1.9	45
122	Termination interference along crystal truncation rods of layered crystals. Journal of Applied Crystallography, 2004, 37, 977-987.	4.5	19
123	Three-dimensional structure of the calcite–water interface by surface X-ray scattering. Surface Science, 2004, 573, 191-203.	1.9	175
124	Mineral–water interfacial structures revealed by synchrotron X-ray scattering. Progress in Surface Science, 2004, 77, 171-258.	8.3	334
125	Interaction of Uranyl with Calcite in the Presence of EDTA. Environmental Science & Technology, 2004, 38, 5078-5086.	10.0	37
126	Orthoclase dissolution kinetics probed by in situ X-ray reflectivity: effects of temperature, pH, and crystal orientation. Geochimica Et Cosmochimica Acta, 2003, 67, 197-211.	3.9	52

Paul Fenter

#	Article	IF	CITATIONS
127	Structures of quartz (100)- and (101)-water interfaces determined by x-ray reflectivity and atomic force microscopy of natural growth surfaces. Geochimica Et Cosmochimica Acta, 2002, 66, 3037-3054.	3.9	115
128	Resolving orthoclase dissolution processes with atomic force microscopy and X-ray reflectivity. Geochimica Et Cosmochimica Acta, 2001, 65, 3459-3474.	3.9	108
129	Quantification of minor phases in growth kinetics experiments with powder X-ray diffraction. American Mineralogist, 2000, 85, 1217-1222.	1.9	11
130	Surface speciation of calcite observed in situ by high-resolution X-ray reflectivity. Geochimica Et Cosmochimica Acta, 2000, 64, 1221-1228.	3.9	244
131	Structure and growth of stearate monolayers on calcite: first results of an in situ X-ray reflectivity study. Geochimica Et Cosmochimica Acta, 1999, 63, 3145-3152.	3.9	55
132	X-ray standing wave study of arsenite incorporation at the calcite surface. Geochimica Et Cosmochimica Acta, 1999, 63, 3153-3157.	3.9	65
133	Alkyl Monolayers on Silicon Prepared from 1-Alkenes and Hydrogen-Terminated Silicon. Journal of the American Chemical Society, 1995, 117, 3145-3155.	13.7	1,093
134	An unexpected packing of fluorinated nâ€alkane thiols on Au(111): A combined atomic force microscopy and xâ€ray diffraction study. Journal of Chemical Physics, 1994, 101, 4301-4306.	3.0	166
135	Medium-energy ion scattering studies of the structure of some reconstructed metal surfaces. Nuclear Instruments & Methods in Physics Research B, 1990, 45, 398-402.	1.4	1
136	Structure of the Cs-induced (1×3) reconstruction of Au(110). Physical Review B, 1989, 39, 5810-5818.	3.2	80